Research Square

Preprints are preliminary reports that have not undergone peer review.
They should not be considered conclusive, used to inform clinical practice,
or referenced by the media as validated information.

Ascorbic acid 2-glucoside priming enhances mesenchymal stem cell-mediated peripheral nerve regeneration through MAPK/ERK-NTF-3 signaling

Chae-Min Ryu
Asan Medical Center
Min-Young Jo
Asan Medical Center
Won Sun Lee
Asan Medical Center
Jae Kwang Kim
orth4535@gmail.com

Asan Medical Center https://orcid.org/0000-0001-5104-4634

Research Article

Keywords: Mesenchymal stem cells, Ascorbic acid 2-glucoside, Priming, Peripheral nerve regeneration, Neurotrophin-3

Posted Date: November 18th, 2026

DOI: https://doi.org/10.21203/rs.3.rs-11587438/v1

License: This work is licensed under a Creative Commons Attribution 4.0 International License.
Read Full License

Ascorbic acid 2-glucoside priming enhances mesenchymal stem cell-mediated peripheral nerve regeneration through MAPK/ERK–NTF-3 signaling

Chae-Min Ryu[1†], Min-Young Jo[2†], Won Sun Lee[3] and Jae Kwang Kim[3*]

[1] Center for Cell Therapy, Asan Medical Center, Seoul, 05505, Republic of Korea

[2] Asan Institute for Life Sciences, Asan Medical Center, Seoul 05505, Republic of Korea

[3] Department of Orthopedic Surgery, Asan Medical Center, University of Ulsan College of Medicine, Seoul, 05505, Republic of Korea

*Corresponding author. E-mail: orth4535@gmail.com

†These authors contributed equally to this work.

Abstract

Background

Peripheral nerve injury (PNI) often results in incomplete nerve regeneration and persistent functional deficits. While mesenchymal stem cell (MSC) therapies offer promise, their clinical translation is hindered by a loss of efficacy after in vitro expansioneclarations and progressive cellular heterogeneity. Priming strategies present a viable solution to enhance regenerative capacity and therapeutic consistency. Furthermore, establishing optimal transplantation dosages and ensuring clinical safety remains critical for successful application.

Methods

To enhance the therapeutic potential of human Wharton's jelly-derived MSCs (hWJ-MSCs) without genetic modification, cultures were primed with an optimized concentration of ascorbic acid 2-glucoside (AA2G). In vitro enhancements were evaluated via proliferation, transwell migration, colony-forming unit-fibroblast (CFU-F), scratch, and neurite outgrowth assays, alongside comprehensive molecular characterizations (Western blotting, qRT-PCR, IF staining, ELISA, and mRNA-seq). In vivo efficacy was assessed using a rat sciatic nerve injury model across two studies: (1) a comparison of Naïve MSCs and AA2G-MSCs, and (2) an evaluation of the dose-dependent effects of AA2G-MSCs. Cells were administered during autologous nerve grafting. Functional and structural recovery was evaluated 16 weeks post-transplantation using gait cycle analysis, joint contracture angle, motor nerve conduction velocity (MNCV), isometric tetanic force testing, and comprehensive histomorphometric analyses of muscle and nerve tissues (H&E, MT, TB staining, and TEM).

Results

AA2G-MSCs exhibited enhanced proliferation, migration, and self-renewal. Transcriptomic and molecular analyses demonstrated that AA2G priming upregulated the neurotrophic factor NTF-3 by activating the MAPK/ERK signaling pathway. In vivo, AA2G-MSC transplantation significantly improved motor recovery and increased muscle mass. Histological evaluations confirmed superior peripheral nerve regeneration in the AA2G-MSC group, characterized by robust axonal remyelination, expanded muscle fiber cross-sectional areas (CSA), and reduced muscle fibrosis. Additionally, the comparative dose analysis successfully established the optimal transplantation dose for maximizing therapeutic outcomes.

Conclusion

AA2G priming effectively promotes peripheral nerve regeneration by enhancing the functional and secretory capacities of hWJ-MSCs. This therapeutic effect is associated with activation of the MAPK/ERK–NTF-3 signaling axis. By identifying an effective transplantation dose and demonstrating robust in vivo efficacy, this study supports AA2G priming as a non-genetic strategy with strong translational potential for advancing MSC-based therapies for PNI.

Keywords

Mesenchymal stem cells, Ascorbic acid 2-glucoside, Priming, Peripheral nerve regeneration, Neurotrophin-3

1. Introduction

Peripheral nerve injury (PNI) often results in slow nerve regeneration and may lead to chronic functional deficits [1]. To promote nerve repair, numerous studies have sought to identify candidate substances that can enhance regeneration [2]. Among various approaches, particular attention has been paid to Schwann cells, which secrete neurotrophic factors, and play a pivotal role in guiding regenerating axons from the proximal nerve stump to their target organs [3]. However, the clinical application of autologous Schwann cells is limited due to the requirement for surgical harvesting of donor nerves and the extended time needed for *in vitro* expansion. These constraints make their use impractical in acute traumatic nerve injuries requiring urgent surgical intervention.

To overcome these limitations, stem cell-based strategies have emerged as

promising alternatives [4]. Mesenchymal stem cells (MSC)-based therapy is considered a promising therapeutic approach for various intractable diseases [5]. MSCs have been shown to promote peripheral nerve regeneration through multiple paracrine effects, including the secretion of neurotrophic factors, and immunomodulation, thereby facilitating axonal regeneration and functional recovery. Various strategies have been proposed to preserve MSC stemness and enhance their regenerative capacity. Ascorbic acid 2-glucoside (AA2G) has been reported to enhance MSC motility and engraftment efficiency without genetic modification, while preserving stemness, increasing antioxidant capacity, and reducing inflammation [6-8]. However, the effects of AA2G on peripheral nerve regeneration and the underlying mechanisms have not yet been elucidated.

Therefore, this study aimed to investigate whether AA2G priming enhances the nerve regenerative potential of MSCs, elucidate the underlying molecular mechanisms, and evaluate the therapeutic efficacy and dose-dependent effects of AA2G-primed MSCs in a peripheral nerve injury model. Elucidating the role of functionally enhanced MSCs may provide insight into the molecular pathways underlying nerve regeneration, facilitate the identification of potential therapeutic targets, and support the clinical translation of optimized MSC-based therapeutic strategies.

2. Materials and methods

2.1. Cell culture and priming

Human mesenchymal stem cells (hMSCs) were obtained from the Cell Therapy Center, Asan Medical Center (Seoul, Korea). All experiments conformed to relevant

guidelines and regulations, and the use of human Wharton's jelly-derived mesenchymal stem cells (WJ-MSCs) was approved by the Institutional Review Board of the Asan Medical Center (No. 2015-0303). hWJ-MSCs were cultured in xeno-free (XF) medium (Welgene, Daegu, Republic of Korea) supplemented with 10% human platelet lysate (hPL; Welgene) and 0.5% gentamicin (Thermo Fisher Scientific, Waltham, MA, USA). All cultures were maintained in a humidified incubator with 5% CO_2 at 37 °C. For AA2G priming, hWJ-MSCs were cultured in medium supplemented with 0.74 mM ascorbic acid 2-glucoside (AA2G; Sigma-Aldrich, St. Louis, MO, USA) for three consecutive passages. Cells cultured under otherwise identical conditions without AA2G supplementation were used as Naïve MSC controls.

2.2. MEK inhibition

To investigate the involvement of MEK/ERK signaling in AA2G-induced effects, AA2G-MSCs were treated with the MEK inhibitor U0126 (#9903; Cell Signaling Technology, Danvers, MA, USA) at 10 μM for 24 h. DMSO-treated AA2G-MSCs were used as vehicle controls.

2.3. Cell differentiation

hWJ-MSCs were cultured in chondrogenic, osteogenic, or adipogenic differentiation medium (Thermo Fisher Scientific) according to the manufacturer's instructions. Chondrogenic differentiation was induced for 7 days, whereas osteogenic and adipogenic differentiation were induced for 21 days. The culture medium was replaced every 3 days throughout the differentiation period. Differentiation was

118 confirmed by cytochemical staining using Alcian Blue for chondrogenesis, Alizarin
119 Red S for osteogenesis, and Oil Red O for adipogenesis (Sigma-Aldrich).
120
121 **2.4. Cell viability**
122 hWJ-MSCs were cultured in the standard growth medium described above, and cell
123 viability was assessed at 5, 24, 48, and 72 h using the EZ-Cytox assay (DoGenBio).
124 Absorbance was measured at 450 nm using a microplate reader.
125
126 **2.5. Scratch assay**
127 After a confluent monolayer was scratched with a sterile scratch tool, the medium
128 was replaced with hPL-free medium. Wound closure was monitored over time, and
129 the wound area was quantified using ImageJ software (National Institutes of Health,
130 Bethesda, MD, USA) at the indicated time points.
131
132 **2.6. Transwell migration Assay**
133 Polycarbonate membranes with an 8 μm pore size were coated with 100 μl of 0.5%
134 gelatin (Sigma-Aldrich, St. Louis, MO, USA) for 1 hour. hWJ-MSCs were
135 resuspended in XF medium (Welgene) supplemented with 0.5% gentamicin (Thermo
136 Fisher) and 0.001% hPL (Welgene) and seeded into the upper chambers of
137 Transwell inserts (Corning Costar). The lower chambers were filled with the same
138 medium supplemented with platelet-derived growth factor-AA (PDGF-AA, 10 ng/ml;
139 R&D Systems, Minneapolis, MN, USA).
140 After 24 hours of incubation, the inserts were removed, and non-migrated cells on

the upper side of the membrane were gently wiped off with cotton swabs. Migrated cells on the underside of the membrane were fixed with 4% paraformaldehyde (PFA) in PBS, washed twice with PBS, and stained with 1% crystal violet solution (Sigma-Aldrich, in PBS). Stained cells were visualized from the lower membrane surface using an EVOS M5000 microscope (Thermo Fisher).

2.7. Colony-Forming Unit-Fibroblast Assay

hWJ-MSCs were cultured for up to 14 days with medium replacement every 3 days. Colonies were stained with 1% crystal violet (Sigma-Aldrich). The number of colonies was then manually counted after colonies were assessed under a light microscope.

2.8. Western blot analysis

The expression of the indicated proteins in hWJ-MSCs was evaluated by western blot using a primary antibody against BDNF (#ab108319; Abcam, Cambridge, UK), HGF (#ab313408), VEGF-A (#ab52917), GDNF (#ab18956), NTF-3 (#704992, Invitrogen, Carlsbad, CA, USA), MEK1/2 (#9122, CST), p-MEK1/2 (#9121, CST), ERK1/2 (#4695, CST), p-ERK1/2 (#9101, CST), and β-actin (#3700, CST). Horseradish peroxidase (HRP)-conjugated anti-rabbit or anti-mouse secondary antibodies (Jackson ImmunoResearch, West Grove, PA, USA) and chemiluminescent reagents (Thermo Fisher) were used for detection

2.9. Gene expression analysis

Total RNA was isolated using RNeasy Mini Kit (Qiagen Inc., Valencia, CA, USA) and

then reverse transcription was performed using TaqMan Reverse Transcription Reagents (Applied Biosystems, Foster City, CA, USA). Quantitative PCR was performed using SYBR Green PCR Master Mix (Bio-Rad) on a QuantStudio Real-Time PCR System (Applied Biosystems). Relative expression levels of target genes were determined using the $2^{-}\Delta\Delta Ct$ method with GAPDH as the endogenous control.

The primers used were as follows: *hBDNF* (forward, GGA ACT CCC AGT GCC GAA CT; reverse, CGC CAG CCA ATT CTC TTT TT), *hHGF* (forward, ACA CCA CAC CGG CAC AAA T; reverse, GCG GGT GTG AGG GTC AAG), *hVEGF-A* (forward, CGA GGG CCT GGA GTG TGT; reverse, TCC TAT GTG CTG GCC TTG GT), *hGDNF* (forward, CAA ATG GCA GTG CTT CCT AGA; reverse, TTA AGA CAC AAC CCC GGT TTT), *hNTF-3* (forward, AGC CGG TGA TTG CAA TGG; reverse, GGA CCC GCG GTG AGT TGT A), and *hGAPDH* (forward, GGA GCG AGA TCC CTC CAA AAT; reverse, GGC TGT TGT CAT ACT TCT CAT GG).

2.10. Neurite outgrowth

NSC-34 cells were cultured in culture medium supplemented with 5% fetal bovine serum (FBS), 50 μg/ml L-ascorbic acid (Sigma-Aldrich), 10 ng/ml brain-derived neurotrophic factor (BDNF), and 10 ng/ml recombinant ciliary neurotrophic factor (CNTF; PeproTech). After 7 days, the medium was replaced with MSC-derived conditioned medium (CdM) and the cells were incubated for 24 h. Then the cells were fixed with 4% PFA and immune stained with an anti-βIII tubulin antibody (ab18207, Abcam). DAPI (4′,6-diamidino-2-phenylindole; D1306, Thermo Fisher Scientific) was used as a counterstain for the cell nuclei. ImageJ software (NIH, Bethesda, MD, USA) was used to quantify neurite length after fluorescence images

were obtained using the EVOS® FL Color Imaging System (Life Technologies).

2.11. Lentiviral shRNA transduction

Short hairpin RNA (shRNA) that targets human NTF-3 (sh*NTF-3*) and scrambled control shRNA were encoded in lentiviral particles that were acquired from VectorBuilder (VectorBuilder Inc., Chicago, Illinois, USA). Prior to lentiviral infection, hWJ-MSCs were plated and allowed to adhere. To improve transduction efficiency, lentiviral particles were transduced into the cells while polybrene was present. After transduction, the fresh XF culture medium was added, and the cells were preserved for further examination.

2.12. Animal model surgical procedure

All animal procedures were conducted in accordance with the guidelines approved by the Institutional Animal Care and Use Committee (IACUC) of Asan Medical Center and Ulsan University College of Medicine (IACUC-2023-20-086). Animal experiments were conducted using a total of 49 adult male and female Sprague-Dawley rats (OrientBio, Gapyong, Gyeonggi-do, Republic of Korea). The animal experiments were conducted in two separate studies. Animals were allocated to three groups (control, Naïve MSCs, and AA2G-MSCs) in the first study and four groups (control, 100K, 250K, and 500K) in the second study, with seven animals per group. Zoletil (20 mg/kg; Virbac Laboratories, Carros, France) was injected intramuscularly into the rats to induce anesthesia before the left sciatic nerve was surgically exposed.

To establish the peripheral nerve injury model, the sciatic nerve was transected,

and a 6-mm nerve segment was excised, reversed, and reimplanted at the original site. The graft was secured to the proximal and distal nerve stumps using 9-0 nylon sutures (Ethicon, Somerville, NJ, USA). In the control group, a total of 20 μL of saline was injected into the epineurium, with 10 μL administered at each of the proximal and distal graft junctions. For the treatment groups, the same total volume of cell suspension containing either Naïve MSCs or AA2G-MSCs was administered in an identical manner. Following transplantation, the skin incision was closed using 4-0 nylon sutures (Ethicon).

2.13. Video gait angle analysis

Video gait analysis was conducted at 8- and 16-weeks post-surgery to evaluate rat joint kinematics. A digital camera was positioned perpendicular to the sagittal plane to capture hindlimb movements, which were assumed to be planar. For this purpose, a custom walking track measuring 1 m in length, 10 cm in width, and 10 cm in height was constructed. Video recordings were obtained using a digital camera (Canon SX730HS, Canon, Tokyo, Japan) placed 1 meter from the track. The camera was calibrated before data acquisition to minimize optical distortion. For each rat, recordings were repeated until a minimum of three satisfactory trials were obtained. Ankle joint angles were measured at maximal plantar flexion during the toe-off phase of the experimental lateral ankle. Manual identification of foot and leg segments in video frames was performed to calculate joint angles, expressed in degrees. Walking trials continued until 3 to 4 consecutive gait cycles without pause were successfully recorded per animal.

2.14. Contracture ankle angle measurement

The contracture ankle angle was evaluated at 16 weeks post-surgery. The angle formed by the anterior border of the tibia and the dorsal aspect of the foot during maximal ankle plantar flexion was measured. The ankle contracture angle was measured on the implanted side, and the extent of recovery from contracture was compared relative to the control group.

2.15. Evaluation of tibialis anterior muscle

Tibialis anterior (TA) muscles were dissected at 16 weeks post-surgery from both the operated and non-operated limbs and weighed on an electronic balance. The weights of TA muscles for each group were photographed and recorded. To compare each group, the weight ratio (%) of the TA muscle was calculated for each animal by dividing the weight of the operated side by that of the non-operated side, and these ratios were compared across groups.

2.16. Isometric tetanic force measurement

To expose and transect the distal tendon of the TA muscle at 16 weeks post-surgery, a separate skin incision was made anterior to the ankle. The knee and ankle joints were immobilized on a custom platform, and the TA tendon was attached to a force transducer using a custom-made clamp. Muscle contractions were evoked by electrical stimulation via a bipolar stimulator (Grass S88, Grass Instruments, Quincy, MA, USA), with stimulation parameters controlled and recorded using LabVIEW software (National Instruments, Austin, TX, USA). All contractions were induced at 4

V to ensure maximal activation of TA motor units. Muscle strength was normalized to the contralateral, non-operated side and expressed as a percentage.

2.17. Analysis of toluidine blue staining

A distal segment of the sciatic nerve (2–3 mm in length from the surgical site) was harvested from each group at 16 weeks post-surgery and fixed in 2.5% glutaraldehyde, followed by post-fixation in 1% osmium tetroxide. The samples were dehydrated through a graded ethanol series and embedded in EPON resin (Miller-Stephenson Chemical Co., Sylmar, CA, USA). For light microscopy, 1-μm-thick transverse sections were prepared and stained with toluidine blue (toluidine blue-O; Daejung Chemicals & Metals, Seoul, Korea). Unbiased random sampling was used to capture digital images of non-overlapping fields at 400× magnification. AxonDeepSeg (ADS), which was implemented in Napari, was used to quantitatively analyze myelinated axons. The TB-stained sections were used to quantify morphometric parameters, including the total number of myelinated axons, axon density, and axonal area.

2.18. Compound muscle action potential measurement

At 8 and 16 weeks following hWJ-MSCs transplantation, rats were anesthetized. Bipolar stimulation electrodes were placed at the sciatic notch to stimulate the sciatic nerve proximal to the nerve graft site. A ground electrode was placed on the tail. For Compound muscle action potentials (CMAP) recording, a pair of electrodes was used, with the active electrode inserted into the tibialis anterior muscle and the reference electrode placed near the achilles tendon. Electrical stimulation was delivered using a stimulus duration of 0.02 ms, and the stimulus intensity was

optimized to the minimal level required to evoke the maximal CMAP response. CMAP were recorded using an electromyography system (Natus Medical Inc., Pleasanton, CA, USA), and the maximal amplitude of the depolarization curve was recorded.

2.19. Histological analysis of TA muscle

At 16 weeks post-transplantation, TA muscles were harvested and fixed in 4% PFA at 4 °C for 24 hours. The fixed tissues were paraffin-embedded and sectioned into 4 μm-thick slices using a microtome. Sections were mounted on slides and stained with hematoxylin and eosin (H&E) and Masson's trichrome (MT; Junsei Chemical). Using an unbiased random sampling method, non-overlapping fields were imaged at 400× magnification. The cross-sectional area (CSA) of muscle fibers and the fibrosis index were quantitatively analyzed using ImageJ software (National Institutes of Health).

2.20. Transmission electron microscopy analysis

Ultrathin sections approximately 60 nm thick were prepared using an ultramicrotome (Ultracut UCT, Leica, Germany). The sections were mounted on 200-mesh grids and stained with 0.2% lead citrate and 1% uranyl acetate. Imaging was performed using a transmission electron microscope (TEM; HT7800, Hitachi, Japan) operated at 80 kV, equipped with a CCD camera. Axon diameters and G-ratios were measured from electron micrographs for each group, and average myelin thickness was calculated accordingly. Myelin thickness measurements and averaging were conducted using

the HITACHI RC16 system based on TEM images.

2.21. Statistical Analysis

The data were statistically analyzed using an unpaired Student's *t*-test, one-way ANOVA, or two-way ANOVA. An unpaired Student's *t*-test was used for comparisons between two independent groups. One-way ANOVA was used for comparisons among multiple groups with a single independent variable, whereas two-way ANOVA was used for analyses involving two independent variables. All statistical analyses were performed using GraphPad Prism 7.0 software (GraphPad Software, La Jolla, CA, USA), and a *p*-value of less than 0.05 was considered statistically significant.

3. Results

3.1. AA2G priming enhances the functional properties of mesenchymal stem cells

To assess the effects of AA2G priming on hWJ-MSCs, AA2G-MSCs were cultured in XF medium supplemented with AA2G, whereas Naïve MSCs were maintained in XF medium without supplementation. Phase-contrast microscopy showed that both Naïve MSCs and AA2G-MSCs retained a typical spindle-shaped, fibroblast-like morphology **(Fig. 1A)**. We next assessed whether AA2G priming affected multilineage differentiation, a fundamental property of MSCs. AA2G-MSCs from all three lots retained their differentiation potential toward chondrogenic, osteogenic, and adipogenic lineages, as demonstrated by Alcian blue, Alizarin Red S, and Oil Red O staining, respectively **(Fig. 1B)**. AA2G-MSCs exhibited enhanced proliferative

capacity **(Fig. 1C)**, increased migratory ability **(Fig. 1D–E)**, and higher colony-forming unit–fibroblast (CFU-F) efficiency **(Fig. 1F)** compared with Naïve MSCs. Collectively, these results indicate that AA2G priming enhances the functional properties of MSCs while preserving their characteristic morphology and multilineage differentiation potential.

3.2. AA2G priming enhances the nerve regenerative potential of mesenchymal stem cells

To evaluate the effects of AA2G priming on the expression of factors associated with nerve regeneration, we examined neurotrophic and angiogenic factors, including brain-derived neurotrophic factor (BDNF), hepatocyte growth factor (HGF), vascular endothelial growth factor (VEGF), glial cell line-derived neurotrophic factor (GDNF), and neurotrophin-3 (NTF-3). Western blot analysis showed increased protein expression of BDNF, HGF, and NTF-3 in AA2G-MSCs **(Fig. 2A and Supplementary Fig. S1)**. qRT-PCR analysis further showed increased mRNA expression of BDNF, HGF, and NTF-3 in AA2G-MSCs compared with Naïve MSCs **(Fig. 2B)** ELISA showed significantly increased secretion of the examined factors in AA2G-MSCs compared with Naïve MSCs **(Fig. 2C)**. We next assessed the effect of conditioned medium derived from AA2G-MSCs (AA2G-MSC-CdM) on neurite outgrowth in NSC-34 cells. AA2G-MSC-CdM significantly increased βIII-tubulin-positive neurite length compared with Naïve MSC-CdM **(Fig. 2D)**. Collectively, these results indicate that AA2G priming enhances the expression and secretion of factors associated with nerve regeneration and promotes neurite outgrowth.

3.3. Transcriptomic analysis reveals activation of MAPK/ERK signaling in AA2G-primed mesenchymal stem cells

RNA sequencing revealed substantial transcriptional changes in AA2G-MSCs compared with Naïve MSCs, with 790 upregulated and 839 downregulated genes **(Supplementary Fig. S2A)**. GO enrichment analysis (Biological Process) identified pathways associated with cell migration, cell proliferation, and response to transforming growth factor beta stimulus **(Fig. 3A).** GSEA further showed significant enrichment of the KEGG MAPK signaling pathway in AA2G-MSCs **(Fig. 3B)**. Heatmap analysis of the leading-edge genes within the enriched MAPK signaling pathway showed distinct expression patterns between AA2G-MSCs and Naïve MSCs **(Supplementary Fig. S2B)**. Volcano plot analysis further showed differential expression of MAPK-related genes, including immediate-early genes, receptor tyrosine kinases, and MAPK kinases **(Fig. 3C)**.

We next examined ERK activation in response to AA2G priming. Western blot analysis showed increased ERK phosphorylation in AA2G-MSCs compared with Naïve MSCs **(Fig. 3D and Supplementary Fig. S3)**. Subcellular fractionation further showed increased p-ERK levels in both the cytosolic and nuclear fractions of AA2G-MSCs, with a more pronounced increase in the nuclear fraction **(Supplementary Fig. S4)**. Consistently, immunofluorescence staining showed an approximately sixfold increase in nuclear p-ERK localization following AA2G priming **(Fig. 3E)**. AA2G priming also significantly increased the expression of ERK-responsive immediate-early genes, including *hFOS*, *hJUND*, *hJUNB*, *hDUSP6*, and *hSRF* **(Supplementary Fig. S5)**. Collectively, these results indicate that AA2G priming activates MAPK/ERK signaling, promotes nuclear accumulation of p-ERK, and enhances the expression of ERK-responsive genes in hWJ-MSCs.

3.4. AA2G enhances nerve regenerative potential through MEK–ERK-mediated

NTF-3 upregulation

To determine whether AA2G-induced ERK activation is mediated by MEK, AA2G-MSCs were treated with a MEK inhibitor (MEKi). MEK inhibition markedly reduced AA2G-induced phosphorylation of both MEK and ERK **(Fig. 4A and Supplementary Fig. 6)** and decreased nuclear p-ERK localization following AA2G priming **(Fig. 4B)**. Consistently, MEKi significantly attenuated the AA2G-induced expression of ERK-responsive immediate-early genes, including hFOS, hJUND, hDUSP6, and hSRF **(Supplementary Fig. S7)**. We next examined whether MEK–ERK signaling regulates NTF-3 expression in AA2G-MSCs. MEKi significantly attenuated the AA2G-induced increase in hNTF-3 mRNA expression and NTF-3 secretion **(Fig. 4C and D)**.

To determine whether NTF-3 contributes to the neurite-promoting effects of AA2G-MSCs, hNTF-3 was knocked down in hWJ-MSCs using lentiviral shRNA. Knockdown of hNTF-3 significantly reduced NTF-3 mRNA and protein expression **(Supplementary Fig. S8A and B)**. Cell proliferation, chemotactic migration, and CFU-F capacity were comparable between shScramble and shNTF-3 MSCs **(Supplementary Fig. S8C–E)**. In contrast, hNTF-3 knockdown significantly attenuated AA2G-CdM-induced neurite outgrowth **(Fig. 4E)**. Collectively, these results indicate that AA2G-induced MEK–ERK activation promotes NTF-3 expression, which contributes to the neurite-promoting effects of AA2G-MSCs.

3.5. AA2G-MSC transplantation improves hindlimb motor function following sciatic nerve injury

A sciatic nerve injury model was used to evaluate whether AA2G-MSCs could enhance nerve regeneration. After transection of a 6-mm segment of the rat sciatic

nerve, the excised segment was rotated 180° and reimplanted as an autograft. The animals were assigned to one of three groups: an untreated control group, a Naïve MSC transplantation group, and an AA2G-MSC transplantation group. In the MSC transplantation groups, cells were locally transplanted into both the proximal and distal sites of the graft **(Fig. 5A)**.

To assess hindlimb functional recovery, we measured the ankle angle during the toe-off (TO) phase of the gait cycle at 8 and 16 weeks postoperatively. At both 8 and 16 weeks, the AA2G-MSC group showed a significantly greater ankle angle than both the control and Naïve MSC groups, whereas no significant differences were observed between the control and Naïve MSC groups **(Fig. 5B and C)**. We further evaluated functional recovery by assessing contracture of the operated hindlimb. At 16 weeks postoperatively, the AA2G-MSC group exhibited significantly greater improvement compared with both the control and Naïve MSC groups **(Fig. 5D and E)**. Collectively, these results indicate that AA2G-MSCs enhance functional recovery after peripheral nerve injury.

To evaluate denervation-induced muscle atrophy and target muscle recovery after sciatic nerve injury, the TA muscle was assessed at 16 weeks postoperatively. The AA2G-MSC group showed a significantly higher TA muscle wet weight ratio than the control and Naïve MSC groups **(Fig. 5F and G)**. Isometric tetanic force of the TA muscle was measured at 16 weeks postoperatively to assess muscle contractile function. The AA2G-MSC group exhibited significantly greater isometric tetanic force than the control and Naïve MSC groups **(Fig. 5H and Supplementary Fig. S9)**. Axonal regeneration and myelination were further evaluated in cross-sections of the regenerated sciatic nerve at 16 weeks postoperatively using toluidine blue (TB)

staining **(Fig. 5I)**. The AA2G-MSC group showed a significantly greater total myelinated axon area, higher myelinated axon count, and higher myelinated axon density than the control and Naïve MSC groups **(Fig. 5J and Supplementary Fig. S10)**. Collectively, these results indicate that AA2G-MSCs enhance target muscle recovery and promote axonal regeneration and myelination after peripheral nerve injury.

3.6. Dose-dependent functional recovery following AA2G-MSC transplantation in a rat sciatic nerve injury model

To evaluate the effects of AA2G-MSC dose on functional recovery, different doses of AA2G-MSCs were transplanted following sciatic nerve injury. Gait analysis showed no significant differences among the groups at 8 weeks. At 16 weeks, the 250K and 500K groups exhibited significantly greater ankle angles than the 100K group **(Fig. 6A and B)**. We further assessed contracture of the operated hindlimb at 16 weeks postoperatively. The 250K group showed a significant improvement compared with the 100K group **(Fig. 6C and D)**. Electrophysiological recovery was assessed by measuring compound muscle action potential (CMAP) amplitudes. Normalized CMAP amplitude relative to the contralateral side increased with increasing AA2G-MSC dose, with significant increases observed from 100K to 250K and from 250K to 500K **(Fig. 6E and F)**. Functional recovery of the TA muscle was further assessed by measuring isometric tetanic force at 16 weeks postoperatively. Isometric tetanic force significantly increased from the control to the 100K group and from the 100K to the 250K group, whereas no significant difference was observed between the 250K and 500K groups **(Fig. 6G and Supplementary Fig. S11)**. Collectively, these results

indicate that increasing the dose of AA2G-MSCs enhances functional and electrophysiological recovery after peripheral nerve injury.

3.7. Dose-dependent effects of AA2G-MSC transplantation on target muscle and sciatic nerve regeneration

To evaluate the effect of AA2G-MSC dose on target muscle recovery, the wet weight ratio of the TA muscle was measured at 16 weeks postoperatively. The 250K group showed a significantly higher TA muscle wet weight ratio than the 100K group, whereas no significant difference was observed between the 250K and 500K groups **(Fig. 7A and B)**. H&E- and Masson's trichrome (MT)-stained cross-sections of the injured TA muscle were used to assess muscle fiber morphology and fibrosis **(Fig. 7C)**. Muscle fiber cross-sectional area (CSA) was significantly greater in the 250K group than in the 100K group, with no significant difference between the 250K and 500K groups and fibrosis was significantly reduced in the 250K group compared with the 100K group, whereas no significant difference was observed between the 250K and 500K groups **(Fig. 7D and E)**.

Axonal regeneration and myelination were further evaluated in cross-sections of the regenerated sciatic nerve using toluidine blue (TB) staining **(Supplementary Fig. S12A)**. Total axon area, axon count, and axon density were significantly greater in the 250K group than in the 100K group **(Fig. 7F and Supplementary Fig. S12B)**. Transmission electron microscopy (TEM) was further used to evaluate myelin ultrastructure **(Fig. 7G)**. Myelin sheath thickness was significantly increased in the 250K group compared with the 100K group, with no significant difference between the 250K and 500K groups **(Fig. 7H)**. The G-ratio was significantly decreased in the 250K group compared with the 100K group, whereas no significant difference was

observed between the 250K and 500K groups **(Fig. 7I)**. Collectively, these results indicate that increasing the AA2G-MSC dose enhances target muscle recovery, axonal regeneration, and myelination following peripheral nerve injury, with substantial regenerative effects observed at the 250K dose and limited additional benefit at the 500K dose.

4. Discussion

AA2G priming enhanced the proliferation, migration, self-renewal capacity, and neurotrophic activity of hWJ-MSCs while preserving their multilineage differentiation potential. Mechanistically, AA2G activated MAPK/ERK signaling and increased NTF-3 expression and secretion, whereas MEK inhibition attenuated these molecular changes. NTF-3 knockdown further abrogated the neurite-promoting activity of AA2G-MSC-conditioned medium. In vivo, AA2G-MSC transplantation significantly improved functional recovery, target muscle preservation, axonal regeneration, and remyelination following sciatic nerve injury. Dose-response analysis further demonstrated substantial regenerative efficacy at 2.5×10^5 cells, with limited incremental benefits at 5.0×10^5 cells for several functional parameters. Collectively, these findings indicate that AA2G priming enhances the regenerative potency of hWJ-MSCs and support its translational potential for peripheral nerve repair.

Enhancing the therapeutic potency of MSCs while maintaining their clinically applicable characteristics remains a critical challenge in stem cell-based therapiesAA2G has previously been reported to enhance wound-healing capacity in BM-MSCs increase antioxidant capacity in human MSCs [6], and maintain stemness in embryonic stem cells and UC-MSCs[7]. However, its functional effects on MSC-

mediated peripheral nerve regeneration under xeno-free culture conditions have not been fully characterized. In the present study, AA2G priming enhanced multiple functional properties of hWJ-MSCs alongside the expression and secretion of key neurotrophic factors. These findings extend previous observations and demonstrate that AA2G priming provides a practical, non-genetic approach for optimizing MSC potency in peripheral nerve repair.

The paracrine activity of MSCs is widely recognized as a major driver of their regenerative efficacy[9]. Previous studies have shown that MSC preconditioning can enrich the secretion of neurotrophic factors, such as NGF and BDNF [10, 11]. Notably, AA2G priming markedly increased NTF-3 expression and secretion in the present study. NTF-3 regulates neuronal survival and axonal growth primarily through TrkC-mediated signaling [12, 13]. Transcriptomic profiling identified significant enrichment of the MAPK signaling pathway in AA2G-MSCs, and molecular analyses confirmed increased ERK phosphorylation, nuclear p-ERK accumulation, and upregulation of ERK-responsive immediate-early genes. MEK inhibition attenuated AA2G-induced NTF-3 upregulation and secretion, whereas NTF-3 knockdown reduced the neurite-promoting effect of AA2G-MSC-conditioned medium. Together, these findings support a mechanistic cascade in which AA2G-induced MEK/ERK activation drives NTF-3 expression and enhances neurotrophic potency. However, this mechanism was established primarily in vitro, and its causal contribution to peripheral nerve regeneration in vivo remains to be confirmed.

In the rat sciatic nerve injury model, AA2G-MSC transplantation yielded superior functional, muscular, and histomorphometric recovery compared with Naïve MSC transplantation. Improvements in gait kinematics and muscle contractile force were

519 accompanied by enhanced target muscle preservation, axonal regeneration, and
520 remyelination, providing complementary functional and structural evidence of nerve
521 repair. The implementation of toe-off (TO) angle analysis provided a quantitative,
522 biomechanically relevant measure of ankle joint dynamics, overcoming key
523 limitations associated with traditional walking-track indices[14],[15]. Taken together,
524 these findings demonstrate that the in vitro functional enhancement induced by
525 AA2G priming successfully translates into superior regenerative efficacy in vivo.

526 Cell dosage is an indispensable consideration for the clinical translation of MSC-
527 based therapeutics, as increasing the cell number does not inherently yield
528 proportional therapeutic gains[16, 17]. In the present study, increasing the AA2G-
529 MSC dose from 1.0×10^5 to 2.5×10^5 cells markedly improved multiple regenerative
530 outcomes, whereas increasing to 5.0×10^5 cells provided limited additional benefits
531 across several measures, despite a dose-dependent rise in CMAP amplitude. Thus,
532 2.5×10^5 cells achieved substantial therapeutic efficacy among the tested doses.
533 Although these findings do not define a definitive minimum effective or absolute
534 optimal dose, they offer valuable preclinical evidence for guiding dose selection in
535 locally administered AA2G-MSC therapies.

536 This study has several limitations. First, although AA2G-induced MAPK/ERK
537 activation was linked to increased NTF-3 expression and neurotrophic activity in
538 vitro, the direct causal role of this pathway in nerve regeneration was not validated in
539 vivo via target-specific loss-of-function models. Second, this study was restricted to a
540 single MSC source (hWJ-MSCs), and whether AA2G priming exhibits comparable
541 efficacy in MSCs from other tissue origins remains to be determined. Third, the dose-
542 response evaluation was conducted across three discrete cell doses and thus cannot

establish a definitive minimum effective dose. Finally, comprehensive safety evaluations including in vivo biodistribution, long-term cell persistence, and tumorigenicity were not conducted. Future studies addressing these aspects will be essential to facilitate clinical translation. Nevertheless, the present findings demonstrate that AA2G priming enhances the regenerative potency of hWJ-MSCs without genetic modification and support its translational potential as an MSC-based strategy for peripheral nerve injury.

5. Conclusion

AA2G priming promotes MSC migration and clonogenic capacity and increased neurotrophic factor expression, particularly NTF-3, through activation of MEK–ERK signaling. Furthermore, AA2G-MSC transplantation improved motor function, muscle recovery, and histological outcomes in a rat sciatic nerve injury model. These findings suggest that AA2G priming represents a promising strategy to enhance MSC-based therapies for peripheral nerve injury.

List of abbreviations

PNI: Peripheral nerve injury

MSCs: Mesenchymal stem cells

AA2G: Ascorbic acid 2-glucoside

XF: Xeno free

NTF-3: Neurotrophin-3

CdM: Conditioned medium

IF: Immunofluorescence

DAPI: 4′,6-diamidino-2-phenylindole

GO: Gene ontology

GSEA: Gene set enrichment analysis

KEGG: Kyoto encyclopedia of genes and genomes

MAPK: Mitogen activated protein kinase

ERK: Extracellular signal regulated kinase

MEK: Mitogen activated protein kinase kinase

TO: Toe off

TB: Toluidine blue

CMAP: Compound motor action potential

H&E: Hematoxylin and eosin

MT: Masson’s trichrome

CSA: Cross sectional area

TEM: Transmission electron microscopy

ANOVA: Analysis of variance

Declarations

Ethics approval and consent to participate

All animal experiments were reviewed and approved by the Animal Care and Use Committee of the Asan Medical Center and Ulsan University College of Medicine. All

procedures were approved by the applicable guidelines and regulation.

Consent for publication

Not applicable

Availability of data and materials

All data generated or analyzed during this study are included in this published article and its supplementary information files.

Competing interests

The authors declare that the research was conducted in the absence of any commercial or financial relationships that could be construed as a potential conflict of interest.

Funding

This work was supported by the Korean Fund for Regenerative Medicine, funded by the Ministry of Science and ICT and the Ministry of Health and Welfare (RS-2023-00215003); the Mid-Career Researcher Program through the National Research Foundation of Korea (NRF), funded by the Ministry of Science and ICT (RS-2025-16066806); the Excellent Young Scientist Research Program through the National Research Foundation of Korea (NRF), funded by the Ministry of Science and ICT (RS-2025-23963487); the Nano & Material Technology Development Program through the National Research Foundation of Korea (NRF), funded by the Ministry of

609 Science and ICT (RS-2025-25441823); and the Asan Institute for Life Sciences,
610 Asan Medical Center (2026IL0022).

611

612 **Author's contributions**

613 C.-M.R: Conceptualization, Methodology, Validation, Formal analysis, Investigation,
614 Data curation, Visualization, Writing – original draft. M.-Y.J: Methodology, Validation,
615 Formal analysis, Investigation, Data curation, Visualization, Writing – original draft,
616 Writing – review & editing. W.S.L: Methodology, Investigation, Formal analysis,
617 Writing – review & editing. J.K.K: Conceptualization, Supervision, Project
618 administration, Funding acquisition, Writing – review & editing. All authors read and
619 approved the final manuscript.

620

621 **Author and Affiliations**

622 Chae-Min Ryu[1†], Min-Young Jo[2†], Won Sun Lee[3] and Jae Kwang Kim[3*]

623 Jae Kwang Kim

624 orth4535@gmail.com

625 Chae-Min Ryu

626 Chaemin0427@amc.seoul.kr

627 Min-Young Jo

628 jom2ny@gmail.com

629 Won Sun Lee

630 dldnjstjs94@gmail.com

[1] Center for Cell Therapy, Asan Medical Center, Seoul, 05505, Republic of Korea

[2] Asan Institute for Life Sciences, Asan Medical Center, Seoul 05505, Republic of Korea

[3] Department of Orthopedic Surgery, Asan Medical Center, University of Ulsan College of Medicine, Seoul, 05505, Republic of Korea

Acknowledgements

Not applicable

6. References

1. Lopes B, Sousa P, Alvites R, Branquinho M, Sousa AC, Mendonca C, Atayde LM, Luis AL, Varejao ASP, Mauricio AC: **Peripheral Nerve Injury Treatments and Advances: One Health Perspective.** *Int J Mol Sci* 2022, **23**.
2. Zhang X, Zhang Y, Chen Y, Ji Y, Lyu Y, Miao Z, Duan X, Liu X: **Unraveling the immune system's role in peripheral nerve regeneration: a pathway to enhanced healing.** *Front Immunol* 2025, **16:**1540199.
3. Madduri S, Gander B: **Schwann cell delivery of neurotrophic factors for peripheral nerve regeneration.** *J Peripher Nerv Syst* 2010, **15:**93-103.
4. Lischer M, di Summa PG, Petrou IG, Schaefer DJ, Guzman R, Kalbermatten DF, Madduri S: **Mesenchymal Stem Cells in Nerve Tissue Engineering: Bridging Nerve Gap Injuries in Large Animals.** *Int J Mol Sci* 2023, **24**.
5. Ferreira LVO, Roballo KCS, Amorim RM: **Mesenchymal stem cell-based therapy for peripheral nerve injuries: A promise or reality?** *World J Stem Cells* 2025, **17:**107833.
6. Ju H, Yun H, Kim Y, Nam YJ, Lee S, Lee J, Jeong SM, Heo J, Kwon H, Cho YS, et al: **Activating transcription factor-2 supports the antioxidant capacity and ability of human mesenchymal stem cells to prevent asthmatic airway inflammation.** *Exp Mol Med* 2023, **55:**413-425.
7. Lee S, Lim J, Lee JH, Ju H, Heo J, Kim Y, Kim S, Yu HY, Ryu CM, Lee SY, et al: **Ascorbic Acid 2-Glucoside Stably Promotes the Primitiveness of Embryonic and Mesenchymal Stem Cells Through Ten-Eleven Translocation- and cAMP-Responsive Element-Binding Protein-1-Dependent Mechanisms.** *Antioxid Redox Signal* 2020, **32:**35-59.
8. Lim J, Heo J, Yu HY, Yun H, Lee S, Ju H, Nam YJ, Jeong SM, Lee J, Cho YS, et al: **Small-sized mesenchymal stem cells with high glutathione**

dynamics show improved therapeutic potency in graft-versus-host disease. *Clin Transl Med* 2021, **11:**e476.
9. Wei S, Dong J, Hu Q, Bai J, Gao X, Shan H, Sheng L, Dai J, Tao L, Yan B, Zhou X: **Advances in mesenchymal stem cells and their derivatives for promoting peripheral nerve regeneration.** *Burns Trauma* 2025, **13:**tkaf027.
10. Pandamooz S, Safari A, Ghorbani N, Jamhiri I, Zare S, Belem-Filho IJA, Dolati P, Salehi MS: **Dimethyl Fumarate Preconditioning can Reinforce the Therapeutic Potential of Bone Marrow Mesenchymal Stem Cells through Trophic Factor Profile Enhancement.** *Adv Biomed Res* 2024, **13:**37.
11. Tolstova T, Dotsenko E, Luzgina N, Rusanov A: **Preconditioning of Mesenchymal Stem Cells Enhances the Neuroprotective Effects of Their Conditioned Medium in an Alzheimer's Disease In Vitro Model.** *Biomedicines* 2024, **12**.
12. Kaplan DR, Miller FD: **Neurotrophin signal transduction in the nervous system.** *Curr Opin Neurobiol* 2000, **10:**381-391.
13. Huang EJ, Reichardt LF: **Neurotrophins: roles in neuronal development and function.** *Annu Rev Neurosci* 2001, **24:**677-736.
14. Varejao AS, Meek MF, Ferreira AJ, Patricio JA, Cabrita AM: **Functional evaluation of peripheral nerve regeneration in the rat: walking track analysis.** *J Neurosci Methods* 2001, **108:**1-9.
15. Wang T, Ito A, Aoyama T, Nakahara R, Nakahata A, Ji X, Zhang J, Kawai H, Kuroki H: **Functional evaluation outcomes correlate with histomorphometric changes in the rat sciatic nerve crush injury model: A comparison between sciatic functional index and kinematic analysis.** *PLoS One* 2018, **13:**e0208985.
16. Galipeau J, Sensebe L: **Mesenchymal Stromal Cells: Clinical Challenges and Therapeutic Opportunities.** *Cell Stem Cell* 2018, **22:**824-833.
17. Moll G, Alm JJ, Davies LC, von Bahr L, Heldring N, Stenbeck-Funke L, Hamad OA, Hinsch R, Ignatowicz L, Locke M, et al: **Do cryopreserved mesenchymal stromal cells display impaired immunomodulatory and therapeutic properties?** *Stem Cells* 2014, **32:**2430-2442.

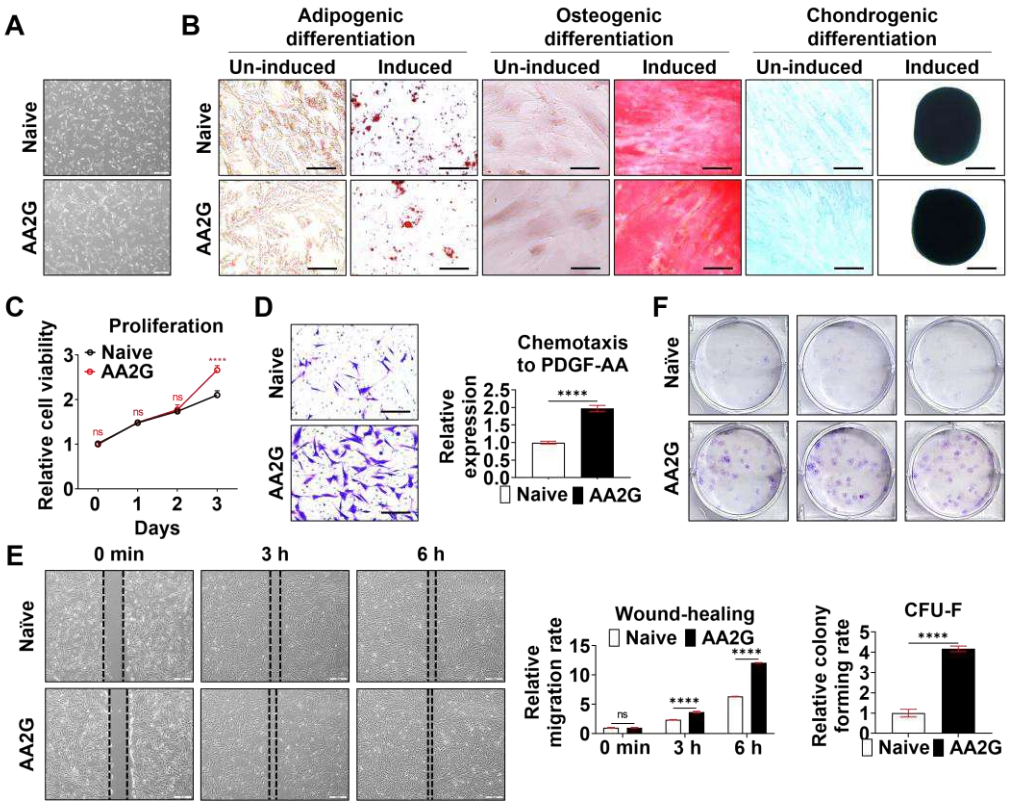


Fig. 1 AA2G priming enhances the functional properties of mesenchymal stem cells. **(A)** Phase-contrast images of Naïve MSCs and AA2G-MSCs. **(B)** In vitro differentiation of Naïve MSCs and AA2G-MSCs into chondrogenic **(**Alcian Blue staining; magnification, ×100; scale bar, 300 μm), osteogenic **(**Alizarin Red S staining; magnification, ×400; scale bar, 75 μm), and adipogenic **(**Oil Red O staining; magnification, ×400; scale bar, 75 μm) lineages. **(C)** Cell proliferation assessed by WST-1 assay. **(D)** Chemotactic migration of Naïve MSCs and AA2G-MSCs assessed by Transwell migration assay (magnification, ×200; scale bar, 150 μm). **(E)** Migratory capacity of Naïve MSCs and AA2G-MSCs assessed by scratch assay over time. **(F)** CFU-F assay to assess colony-forming capacity. Quantitative data are presented as mean ± SEM. Statistical significance was determined by unpaired Student's *t*-test and two-way ANOVA (n.s. = not significant, ****$p < 0.0001$ versus the Naïve MSC group).

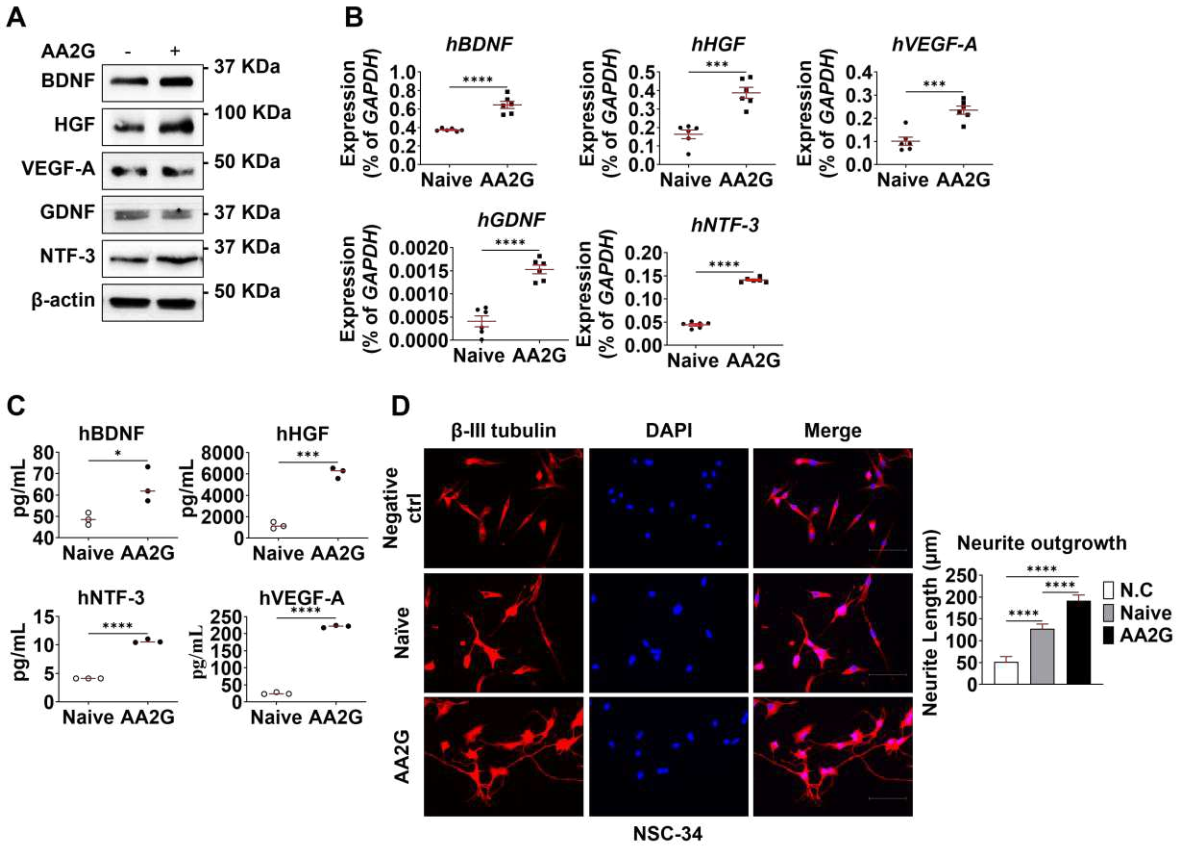


Fig. 2 AA2G priming enhances the nerve regenerative potential of mesenchymal stem cells. **(A)** Protein expression levels of neurotrophic and angiogenic factors in Naïve MSCs and AA2G-MSCs were assessed by Western blot analysis. **(B)** mRNA expression levels of neurotrophic and angiogenic factors in Naïve MSCs and AA2G-MSCs were assessed by qRT-PCR. **(C)** Secreted protein levels in CdM derived from Naïve MSCs and AA2G-MSCs were measured by ELISA. **(D)** Immunofluorescence staining for βIII-tubulin in NSC-34 cells cultured with CdM derived from Naïve MSCs or AA2G-MSCs (magnification, ×400; scale bar, 75 μm). Quantitative data are presented as mean ± SEM. Statistical significance was determined by unpaired Student's *t*-test and two-way ANOVA (n.s. = not significant, **p* < 0.05, ****p* < 0.001, *****p* < 0.0001 versus the Naïve MSC group).

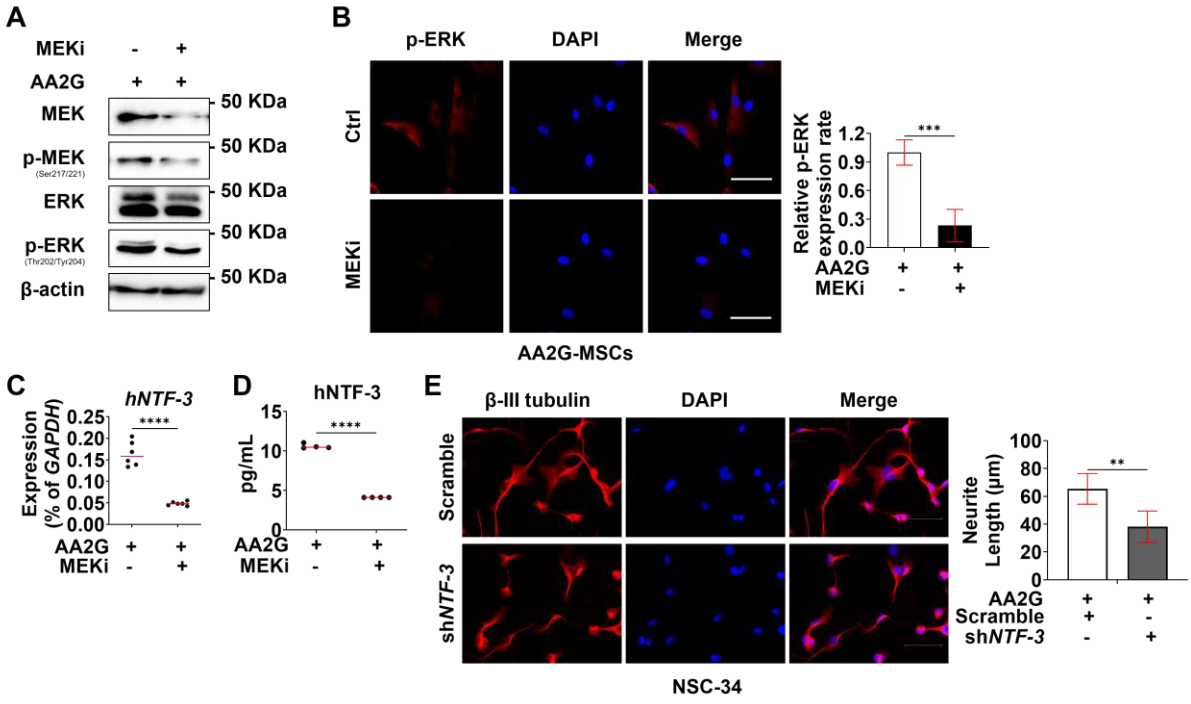


Fig. 3 Transcriptomic analysis reveals activation of MAPK/ERK signaling in AA2G-primed mesenchymal stem cells. (A) GO enrichment analysis of DEGs. Dot size represents gene count, and color indicates statistical significance. **(B)** GSEA of the KEGG MAPK signaling pathway in AA2G-MSCs compared with Naïve MSCs. **(C)** Volcano plot of differentially expressed genes between Naïve MSCs and AA2G-MSCs. Significant DEGs were defined as $|\log_2 FC| \geq 0.585$ and $p < 0.05$. **(D)** Western blot analysis of ERK1/2 and p-ERK1/2 in Naïve MSCs and AA2G-MSCs. **(E)** Immunofluorescence staining of p-ERK in Naïve MSCs and AA2G-MSCs (magnification, ×400; scale bar, 75 μm). Quantitative data are presented as mean ± SEM. Statistical significance was determined by unpaired Student's *t*-test (****$p <$ 0.0001 versus the Naïve MSC group).

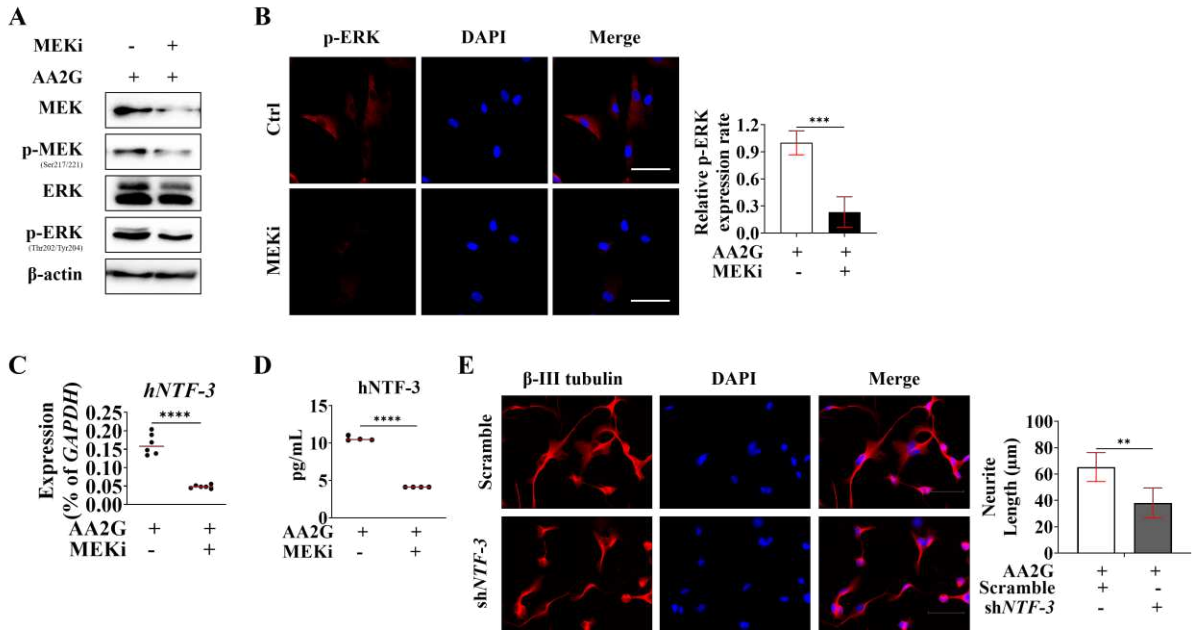


Fig. 4 AA2G enhances nerve regenerative potential through MEK–ERK-mediated NTF-3 upregulation. (A) Western blot analysis of MEK, p-MEK, ERK1/2, and p-ERK1/2 in AA2G-MSCs with or without MEK inhibitor (MEKi; U0126) treatment. **(B)** Immunofluorescence staining of p-ERK in AA2G-MSCs with or without MEKi treatment (magnification, ×400; scale bar, 75 μm). **(C)** RT-qPCR analysis of *hNTF-3* expression in AA2G-MSCs with or without MEKi treatment. **(D)** ELISA measurement of secreted NTF-3 in AA2G-MSCs with or without MEKi treatment. **(E)** Neurite outgrowth of NSC-34 motor neuron-like cells cultured with conditioned medium derived from AA2G-MSCs transduced with shScramble or shNTF-3 (magnification, ×400; scale bar, 75 μm). Quantitative data are presented as mean ± SEM. Statistical significance was determined by unpaired Student's *t*-test and two-way ANOVA (**$p < 0.01$, ***$p < 0.001$, ****$p < 0.0001$ versus AA2G-MSCs or AA2G-MSCs transduced with shScramble).

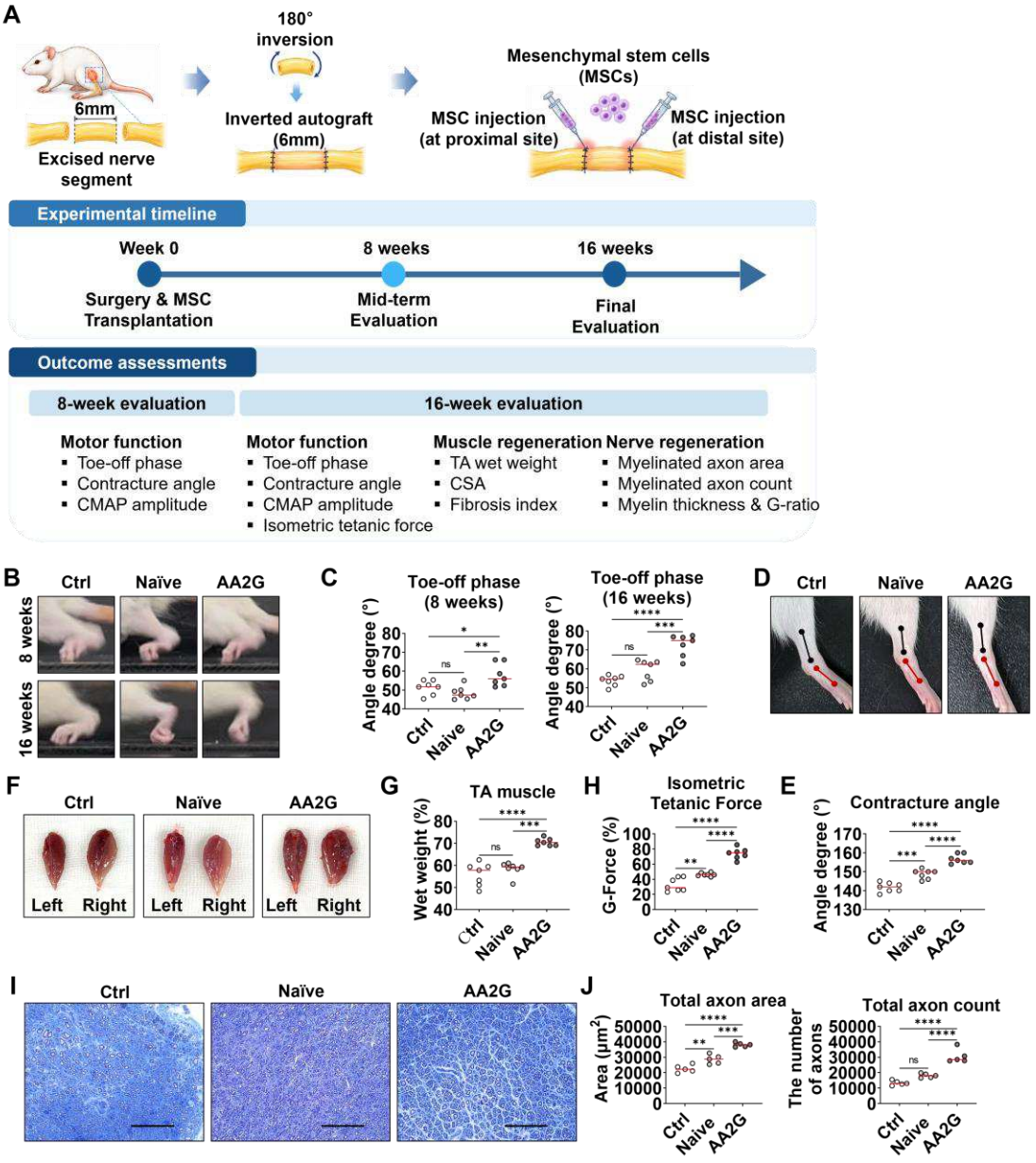


Fig. 5 AA2G-MSC transplantation enhances functional recovery and nerve regeneration following sciatic nerve injury. (A) Schematic diagram of preclinical studies of MSC therapy. **(B–C)** Gait analysis to assess the ankle angle during the TO phase at 8 and 16 weeks postoperatively. **(D–E)** Contracture angle measurement at 16 weeks postoperatively, assessed by passive extension of the operated hindlimb. **(F–G)** TA muscle wet weight ratios are quantified in representative images of TA muscles taken from the operated (left) and unoperated (right) limbs 16 weeks

postoperatively. **(H)** Isometric tetanic force of the TA muscle measured to assess muscle contractile function. **(I)** TB-stained semi-thin cross-sections of regenerated sciatic nerves (magnification, ×400; scale bar, 75 μm). **(J)** Quantitative histomorphometric analysis of total myelinated axon area, and myelinated axon count. Quantitative data are presented as mean ± SEM. Statistical significance was determined by one-way ANOVA (n.s. = not significant, *$p < 0.05$, **$p < 0.01$, ***$p < 0.001$, ****$p < 0.0001$ versus control and Naïve MSC groups).

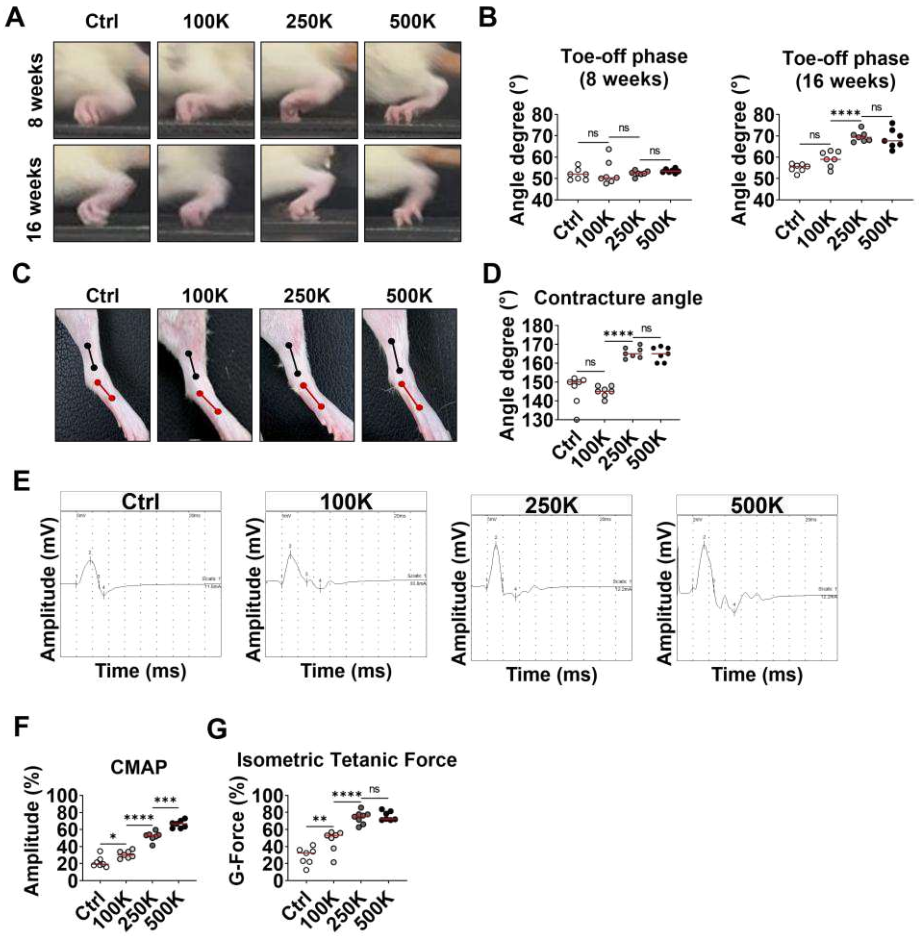
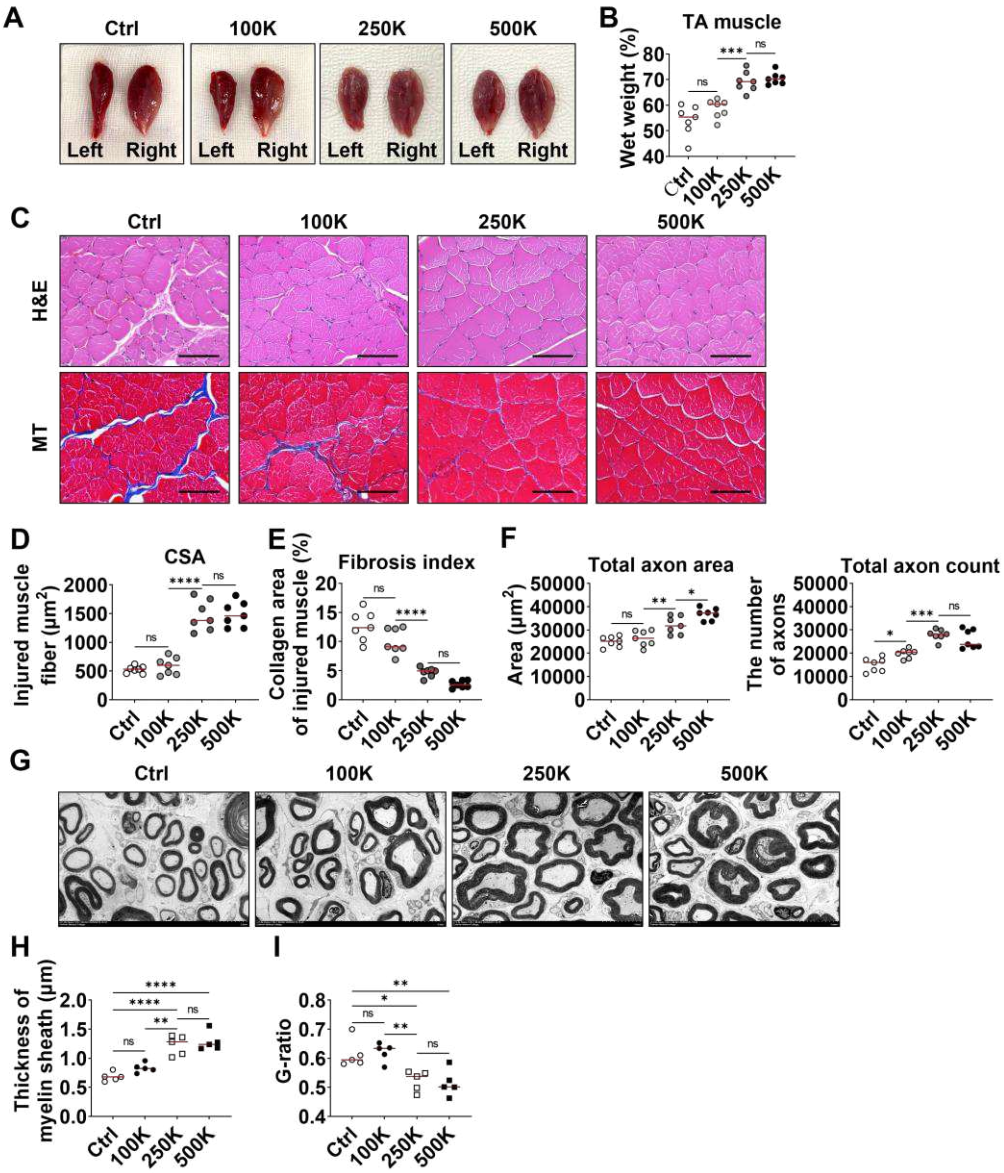


Fig. 6 Dose-dependent functional recovery following AA2G-MSC transplantation in a rat sciatic nerve injury model. (A–B) Ankle angle measured during the TO phase of the gait cycle at 8 and 16 weeks postoperatively. **(C–D)** Contracture angle measured at 16 weeks postoperatively by passive extension of the operated hindlimb. **(E–F)** CMAP amplitude recorded from the tibialis anterior muscle following sciatic nerve stimulation at 16 weeks postoperatively. **(G)** Isometric tetanic force of the TA muscle measured at 16 weeks postoperatively. Quantitative data are presented as mean ± SEM. Statistical significance was determined by one-way ANOVA (n.s. = not significant, *$p < 0.05$, **$p < 0.01$, ***$p < 0.001$, ****$p < 0.0001$ for comparisons between adjacent dose groups).



780

781 **Fig. 7. Dose-dependent effects of AA2G-MSC transplantation on target muscle**
782 **and sciatic nerve regeneration. (A–B)** TA muscle wet weight ratios are quantified
783 in representative images of TA muscles taken from the operated (left) and
784 unoperated (right) limbs 16 weeks postoperatively. **(C–E)** Representative H&E- and
785 MT-stained cross-sections of injured TA muscles used for myofiber CSA and fibrotic
786 area analysis (magnification, ×400; scale bar = 75 μm). **(F)** Quantitative
787 histomorphometric analyses of total axon area, and axon count in regenerated
788 sciatic nerves. **(G)** Representative TEM images of regenerated sciatic nerves

(magnification, ×11,000; scale bar, 5 μm). Quantitative analyses of myelin ultrastructure, including **(H)** myelin sheath thickness and **(I)** G-ratio**.** Quantitative data are presented as mean ± SEM. Statistical significance was determined by two-way ANOVA (n.s. = not significant, *$p < 0.05$, **$p < 0.01$, ***$p < 0.001$, ****$p < 0.0001$ for comparisons between adjacent dose groups).

Supplementary Files

This is a list of supplementary files associated with this preprint. Click to download.

- AdditionalFigure1.tif
- AdditionalFigure10.tif
- AdditionalFigure11.tif
- AdditionalFigure12.tif
- AdditionalFigure2.tif
- AdditionalFigure3.tif
- AdditionalFigure4.tif
- AdditionalFigure5.tif
- AdditionalFigure6.tif
- AdditionalFigure7.tif
- AdditionalFigure8.tif
- AdditionalFigure9.tif
- Coverletter.docx